

# Nonlinear Control and Implementation of a Hybrid Power System

Masoud Bahmanpour \*, Hamid Reza Koofigar \*\*, Majid Delshad \*\*\*, Mohammad Hasan Tosifian \*

\* Department of Electrical Engineering, Saveh Branch, Islamic Azad University, Saveh, Iran.

\*\* Department of Electrical Engineering, University of Isfahan, Isfahan, Iran.

\*\*\* Department of Electrical Engineering, Isfahan (Khorasgan) Branch, Islamic Azad University, Isfahan, Iran.

\*\* (P.O.B. 8174673441, corresponding author e-mail: koofigar@eng.ui.ac.ir)

---

**Abstract:** In this paper, the maximum power point tracking (MPPT) and the load voltage control of a Hybrid Power System (HPS) has been investigated. The underlying HPS consists of a boost converter, a Bidirectional DC-DC converter (BDC), a photovoltaic (PV) panel, and a battery. The integral sliding mode controller (ISMC) is proposed For MPPT. The load voltage control system is based on the use of a double-loop controller, an inner one to control the current of the battery by the sliding mode control (SMC) and the outer one to control the load voltage by a PI controller. Dynamic equations of the system are derived from the “state-space averaging method”. Afterwards, a method for obtaining the load resistance is presented to improve the dynamic response. Then, the results of the proposed controllers for MPPT and the load voltage control by means of simulations using the Matlab/Simulink software are discussed. The experimentally derived results, by implementation on SPARTAN XC3S400 chip, are also given for justification.

**Keywords:** Maximum Power Point Tracking (MPPT), Hybrid Power System (HPS), Photovoltaic (PV), Load resistance, Integral Sliding mode control (ISMC), Double-loop controller.

---

## 1. INTRODUCTION

Currently, renewable energy is receiving greater attention as a sustainable alternative to more traditional energy sources. One of these environmentally-friendly energy sources is solar energy. The application of photovoltaic arrays in stand-alone systems has become popular due to some advantages, as low upkeep cost, low maintenance, no waste or byproducts, and easy expansion by using multiple solar panels and batteries. The problem of harnessing solar energy is that solar panels cannot produce power steadily because their power output rates change with days and hours (Thounthong, 2011; Sauer, 2015).

Hybrid power sources (HPSs) are designed to generate power more efficiently (Mojallizadeh and Badamchizadeh, 2016). DC-DC converters are one of the key elements in HPSs: They interface between the power sources and other parts of a hybrid system. Control of DC-DC converters is necessary for HPS. There are two challenges to control the HPS system. One, extracting the MPPT from PV module and the other, the load voltage regulation. Several studies have been carried out in the field of MPPT methods. Among these methods, perturb and observe (P&O) (Elgendy et al., 2015; Killi and Samanta, 2015; Ahmed and Salam, 2016) and incremental conductance (INC) (Xu et al., 2015; Bahmanpour et al., 2018) are widely used in the literature, but they fail under fast varying climatic conditions (Ghassami, 2013) and have no robustness properties. There are also other techniques such as, adaptive control (El Fadil and Giri, 2011; Koofigar, 2016), neural networks (Syafaruddin et al., 2012), fuzzy logic (Algazar et al., 2012), SMC (Belkaid et al., 2016; Mojallizadeh and Karimi,

2014), fractional short circuit current method (Sher et al., 2015) which estimates the optimal current by short circuit current and fractional open circuit voltage method (Murtaza et al., 2012) which estimates the optimal voltage by open circuit voltage. The last two methods are very simple, but they have a weaker and less accurate performance. Recently, the problem of controlling HPS has been studied and researched. The APBC controller has designed by using algebraic parameter identification (Mojallizadeh and Badamchizadeh, 2016; Tofighi and Kalantar, 2011). In the method introduced, regarding the algorithm, the control signal cannot be followed by rapid changes, whole the changes must be slow, so the dynamic response of the system is slow and is accompanied by a large overshoot. The SMC is used for this purpose (Mojallizadeh and Karimi, 2014a; Mojallizadeh and Karimi, 2014b; Khabbazi et al., 2017), but the problem that ensues is that power losses such as loss of inductors and losses of power switches in the converters are not considered; therefore, this causes undesirable control of the system in operation.

The purpose of this paper is to design two control signals. The first control signal is applied to the boost converter for the MPPT of the PV array, and the second control signal is applied to the BDC to guarantee the stability and adjust the output voltage to the desired value. To this end, the boost converter is driven with ISMC and BDC is driven with a two-loop controller, an outer one to control the load voltage by a PI controller and the inner one to control the current of the battery by the SMC. Then, to improve the dynamic response of the system, a method for obtaining the load resistance is presented.

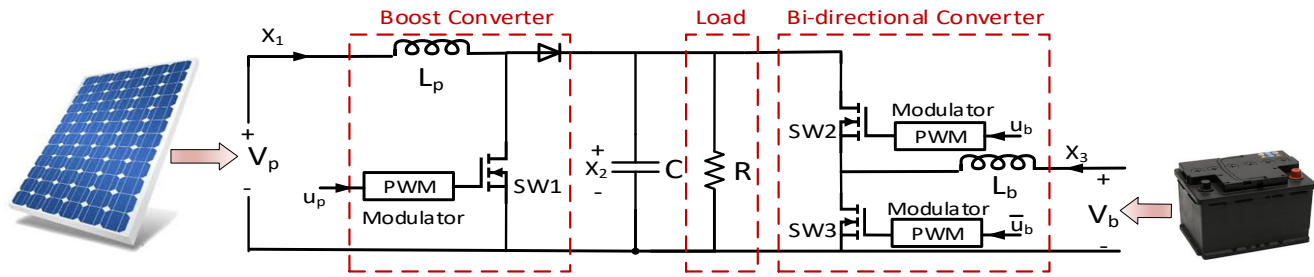


Fig. 1. Circuit diagram of HPS.

This paper is organized as follows: The converters are modeled in Section 2; The proposed controllers are designed in Section-3; The results of the simulations and experiments are given in Sections 4 and 5; and conclusions are presented in Section 6, respectively.

## 2. HPS MODELING

The circuit modules of an HPS are schematically shown in Fig. 1. It consists of a PV panel, a battery and interfacing DC-DC converters, i.e., a BDC and a boost converter.

### 2.1 Mathematical model of DC-DC converters

By utilizing the state-space averaging method (Emadi, 2004), dynamic equations of the system can be expressed as:

$$\begin{cases} L_p \dot{x}_1 = V_p - R_{lp} x_1 - V_d - x_2 - (R_{sw1} x_1 - V_d - x_2) u_p \\ C \dot{x}_2 = -\frac{x_2}{R} + x_1 (1 - u_p) + x_3 u_b \\ L_b \dot{x}_3 = V_b - (R_{lb} + R_{sw3}) x_3 - x_2 u_b \end{cases} \quad (1)$$

where  $L_p$  and  $L_b$  denote the inductances,  $R_{lb}$  and  $R_{lp}$  denote the resistance of the inductors  $L_b$  and  $L_p$ , respectively,  $C$  is the capacitor,  $R$  is the load resistance,  $R_{sw1}$  and  $R_{sw3}$  denote the conductive resistances of the switches  $SW1$  and  $SW3$ ,  $V_d$  is forward voltage of the diode,  $V_b$  denotes the battery voltage and  $V_p$  is the voltage of the PV panel.  $X = [x_1, x_2, x_3]^T$  is the state vector which includes current of the PV panel ( $I_p$ ), load voltage ( $V_C$ ) and battery current ( $I_b$ ), respectively. The control inputs  $0 \leq u_p \leq 1$  and  $0 \leq u_b \leq 1$  are the duty cycle of the switches  $SW1$  and  $SW2$ , respectively ( $SW3$  acts in the opposite direction of  $SW2$ ).

### 2.2 Mathematical model of the battery

Storage devices are utilized for energy storage in HPS. The battery store energy in the electrochemical form. The battery is modelled based on the generic Thevenin model (Lin, 2000). Fig. 2 shows equivalent circuit of the battery, where  $V_{boc}$  is the open circuit voltage and  $r_b$  is the equivalent resistance.

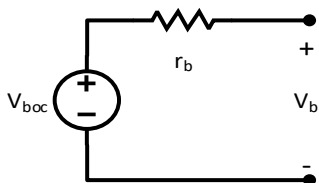


Fig. 2. Equivalent circuit of the battery storage.

### 2.3 Mathematical model of the PV array

Different models based on the PV cell are used to explain this effect. The one-diode model (Azzouzi, 2013; Ahmad, 2014) or the two-diode model (Petcut, 2010; Dragomir et al., 2010) are usually considered. The single diode model (fig. 3) is the most classical model described in the literature, in which the simplest model can be represented by a current source in antiparallel with a diode and the non-idealities are represented by the insertion of the resistances  $R_s$  (series resistance) and  $R_p$  (parallel resistance).

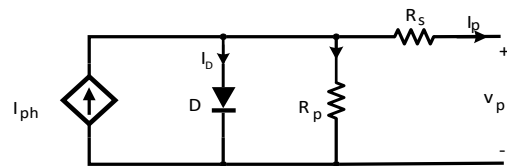


Fig. 3. Equivalent model of the PV panel.

The PV panel simulation model is based on the output current of one PV equivalent model, and its mathematical equation (Park et al., 2016) is represented by:

$$I_p = I_{ph} - I_{rs} \left( e^{\frac{q(V_p + I_p R_s)}{A k_b T}} - 1 \right) - \frac{(V_p + I_p R_s)}{R_p} \quad (2)$$

$$I_{ph} = \frac{\lambda}{1000} [I_{scr} + k_I (T - T_r)] \quad (3)$$

$$I_{rs} = I_{or} \left( \frac{T}{T_r} \right)^3 e^{\frac{q E_g}{k_b A} \left( \frac{1}{T_r} - \frac{1}{T} \right)}. \quad (4)$$

Where  $V_p$  and  $I_p$  are the PV cell voltage and current, respectively,  $I_{rs}$  is the diode reverse saturation current,  $q$  is the electron charge ( $1.6 \times 10^{-19}$  coulomb),  $A$  is the ideality factor of the p-n junction (1.12),  $k_b$  is the Boltzmann constant ( $1.3805 \times 10^{-23}$  J/K),  $\lambda$  is Solar irradiance level (0~1000 W/m<sup>2</sup>),  $k_I$  is the temperature coefficient ( $12 \times 10^{-4}$  A/K),  $T$  is the cell temperature,  $T_r$  is the reference temperature (298°K),  $E_g$  is the bandgap energy (1.2eV),  $I_{or}$  is the saturation current at  $T_r$  ( $5.98 \times 10^{-8}$  A), and  $I_{scr}$  is the short circuit current (1.45 A). In Figs. 4 and 5, the power characteristics of the analyzed PV cell, considering solar irradiation and temperature changes, are shown. The curves show clearly the nonlinear characteristics, and they are strongly influenced by climate changes. Thus, it becomes necessary to use techniques to extract the maximum power from these panels. The requirement for maximum power point tracking (MPPT) is

raised by the fact that the MPP of the PV panel continuously varies with temperature and illumination changes.

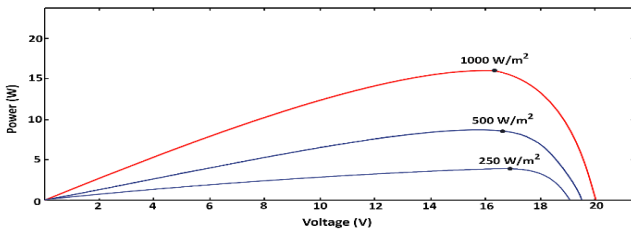


Fig. 4. PV power characteristic for different irradiation levels.

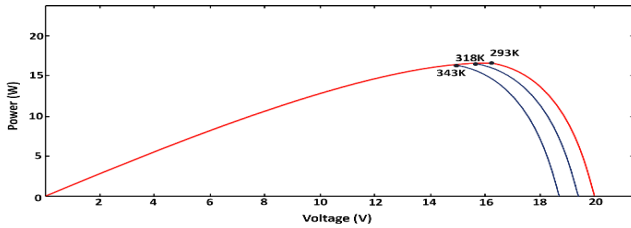


Fig. 5. PV power characteristic for different temperature levels.

### 3. CONTROLLER DESIGN

The goal of the controller is to produce two control signals with a feasible amplitude, including  $u_p$ , applied to the boost converter for MPPT of the PV panel, and  $u_b$ , applied to the BDC to adjust the load voltage to the desired value, to face rapid power vacillations.

#### 3.1 MPPT Controller Designer

In the conventional SMC (Belkaid et al., 2016; Mojallizadeh and Karimi, 2014; Khabbazi et al., 2017) by using Fig.4 under uniform insolation conditions and selecting the PV sliding surface as (5), it is guaranteed that the system state will hit the surface and produce maximum power persistently.

$$s_p = \frac{dp_{pv}}{dv_p} = x_1 + v_p \frac{dx_1}{dv_p} = 0 \quad (5)$$

where  $p_{pv}$  is the PV power. Finally, the conventional control signal is obtained:

$$u_p = 1 - \frac{v_p}{x_2} + ks_p. \quad (6)$$

MPPT is based on SMC, which was presented previously, has the following advantages.

- 1) Unlike SMC, the conventional algorithms have complicated mathematical relationships and if-then conditions, so it is difficult to implement them.
- 2) Unlike SMC, common control methods like the APBC required reference current ( $x_{1d}$ ) for control law synthesis.

But the problem that can be taken with the conventional SMC is that the boost converter elements such as the inductor ( $L_p$ ) are ideally considered; Consequently, the controller cannot tracking MPP in reality. To solve this problem, ISMC is proposed:

$$u_p = 1 - \frac{v_p}{x_2} + ks_p + k_i \int s_p dt \quad (7)$$

where  $k$  and  $k_i$  are constant coefficients and are determined by trial and error method by using computer simulations. The block diagram of proposed method is shown in Fig. 6.

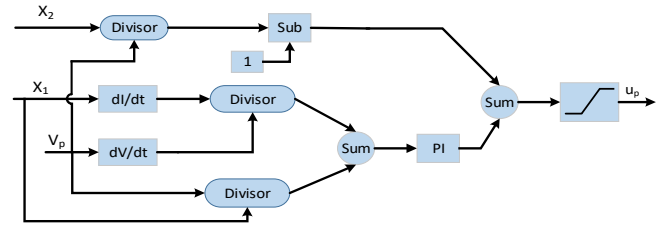


Fig. 6. Implementation of ISMC method.

#### 3.2 PI-SMC Design

Two PI control loops to control the hybrid system is used and then the double-loop controller, an inner one to control the current of the battery by the SMC and the outer one to control the load voltage: by a PI controller, are used for the same system (Etxeberria, 2011). This structure can be named as PI-SMC and shown in Fig. 7. The results show that the PI based control system is not able to maintain its good response when the operation point is not inside a limited range around the operating point selected to design the controllers. Due to the characteristics of the HPS and the microgrid operation, the PI based controller cannot assure the stability of the system in the entire operation range. The PI-SMC shows a higher robustness and it is able to operate correctly at the different cases that have been analyzed.

A PI controller has been used to adjust the load voltage to the desired value. Control law is shown below (8). Its values  $K_{p1}$  and  $K_{i1}$  are shown in table 1.

$$x_{3d} = -(K_{p1}(x_2 - x_{2d}) + K_{i1} \int (x_2 - x_{2d})dt). \quad (8)$$

A nonlinear controller has been designed in order to analyze its advantages compared to the linear controller. The SMC has been selected due to its ability to guarantee stability and robustness against uncertainties (Tan et al., 2008).

Voltage regulation sliding surface ( $s$ ) is selected as:

$$s = x_3 - x_{3d} \quad (9)$$

in order to get the equivalent control ( $u_{eq}$ ), the equivalent control is determined from the following condition:

$$\dot{s} = \frac{\partial s}{\partial x_1} \dot{x}_1 + \frac{\partial s}{\partial x_2} \dot{x}_2 + \frac{\partial s}{\partial x_3} \dot{x}_3 = 0. \quad (10)$$

The equivalent control is then derived:

$$u_{eq} = \frac{v_b - (R_{lb} + R_{sw3})x_3}{x_2}. \quad (11)$$

The step for obtaining  $(R_{lb} + R_{sw3})x_3$  is described in Section 3. If  $u_b = 1$  as a result  $(R_{lb} + R_{sw3})x_3$  can not be obtained. The real control signal is proposed as:

$$u_b = \begin{cases} 0 & u_{eq} + k_s s \leq 0 \\ u_{eq} + k_s s & 0 < u_{eq} + k_s s < 0.95 \\ 0.95 & 0.95 \leq u_{eq} + k_s s \end{cases} \quad (12)$$

where  $k_s$  is a constant coefficient and is determined by trial and error methods using computer simulations.

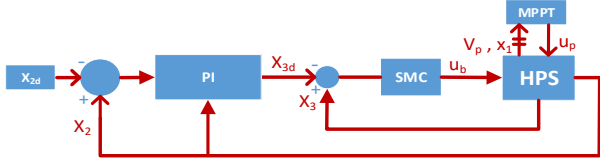


Fig. 7. Structure of PI-SMC.

The existence of the approaching mode of the proposed sliding function is provided. A Lyapunov function is a positive definite term and is defined here as:

$$V = \frac{1}{2} s^2. \quad (13)$$

The time derivative of  $V$  can be written as:

$$\dot{V} = 1/2 s \dot{s}. \quad (14)$$

The achievability of  $s = 0$  will be obtained by  $\dot{V} < 0$ .  $\dot{V}$  can be written as follows:

$$\dot{V} = s(V_b - (R_{lb} + R_{sw3})x_3 - x_2 u_b) \quad (15)$$

assumptions:  $x_2 > v_b > 0, k_s > 0$ .

Three cases should be examined for the fulfillment of  $\dot{V} < 0$ .

Case I: when  $u_b = 0$

$$\dot{V} = s(V_b - (R_{lb} + R_{sw3})x_3) \quad (16)$$

in this case  $x_3$  is rising, as a result  $L_b \dot{x}_3 > 0$ , by replacing it into (1) we have  $V_b - (R_{lb} + R_{sw3})x_3 > 0$  and according to  $u_{eq} + k_s s \leq 0$ , by replacing (11) it into and with assumptions, the sign of (s) is negative, as a result,  $\dot{V}$  is negative definite.

Case II: when  $0 < u_b < 0.95$

by finding  $u_b$  from (12) and replacing (11) and (15), we have:

$$\dot{V} = -k_s x_2 s^2 \quad (17)$$

by assumptions,  $\dot{V}$  is negative definite.

Case III: when  $u_b = 0.95$

$$\dot{V} = s(V_b - (R_{lb} + R_{sw3})x_3 - 0.95x_2) \quad (18)$$

in this case  $x_3$  is falling, as a result  $L_b \dot{x}_3 < 0$ , by replacing it into (1) we have  $V_b - (R_{lb} + R_{sw3})x_3 - 0.95(x_2) < 0$  and according to  $u_{eq} + k_s s \geq 0.95$ , by replacing (11) it into and with assumptions, the sign of (s) is positive, as a result,  $\dot{V}$  is negative definite. From the discussion above, the stability of the system can be guaranteed using the proposed control law (12).

### 3.3 PI (propose)-SMC Design

According to the HPS, we have:

$$P_b + P_{pv} = P_L + P_{loss} \quad (19)$$

$$x_3 = \frac{1}{v_b} \left( \frac{x_{2d}^2}{R} - v_p x_1 \right) + \frac{P_{loss}}{v_b} \quad (20)$$

where  $P_b, P_{pv}, P_L$  and  $P_{loss}$  are battery power, PV power, load power, and power losses respectively. To improve the dynamic response of the system, the PI control law is shown below (21).

$$x_{3d} = \frac{1}{v_b} \left( \frac{x_{2d}^2}{R} - v_p x_1 \right) - k_{p1}(x_2 - x_{2d}) - k_{i1} \int (x_2 - x_{2d}) dt. \quad (21)$$

In fact, with this choice, the current designed for the battery can be changed faster with power variations. The PWM signals SW1 and SW2, load voltage ( $x_2$ ) and battery current ( $x_3$ ) in all of the possible modes of operation HPS (mode a: SW1= open and SW2= close, mode b: SW1= open and SW2=open, mode c: SW1=close and SW2= close, mode d: SW1=close and SW2=open) are shown in Fig. 8. In the mode (d) where SW1=close and SW2=open, capacitor (C) is discharged through the load resistor and the value of R can be measured. We have the capacitance discharge equation:

$$R = - \frac{t_R}{C(\ln x_2(t_R) - \ln x_2(0))} \quad (22)$$

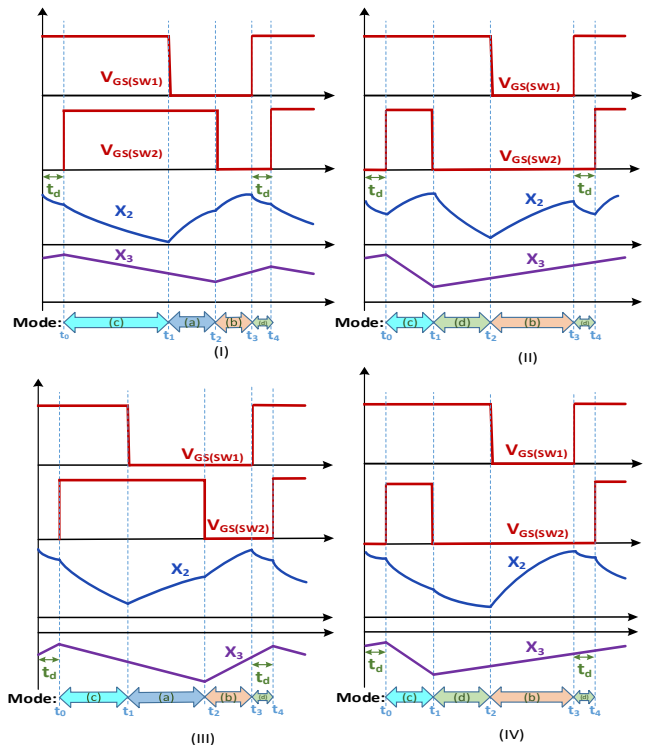


Fig. 8. Key operation waveforms of the proposed HPS when operating in (I)  $u_p < u_b, x_3 > 0$ , (II)  $u_p > u_b, x_3 > 0$ , (III)  $u_p < u_b, x_3 < 0$ , (IV)  $u_p > u_b, x_3 < 0$ .

where  $x_2(t_R)$  is the Capacitor voltage at time  $t_R$ ,  $x_2(0)$  denotes the initial voltage of the capacitor and  $t_R$  is the time at which

the capacitor voltage ranged verb from  $x_2(0)$  to  $x_2(t_R)$ . This mode is shown in Fig. 9.

To calculate R, it is necessary to create a delay of  $t_d$  size between the two PWM signals SW1 and SW2. If there is no delay, R may not be calculated. For example, in Fig. 8. (I) and 8. (III), if not delayed ( $t_d$ ), R cannot be calculated because SW1=close and SW2=open, does not occur.  $t_R < t_d$  shown in Fig. 9, because there will be a small spark in the load voltage and current on the rising and falling edge of the pulses.

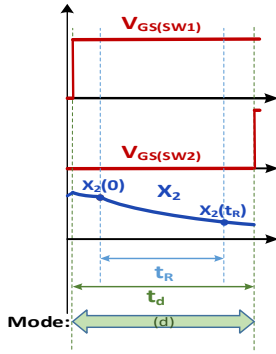


Fig. 9. Demonstration of mode (d) for R calculating.

In the mode (d) or (b) where sw2=open, for calculating  $(R_{lb} + R_{sw3})x_3$ , we have:

$$(R_{lb} + R_{sw3})x_3 = V_b - L_b \left[ \frac{x_3(t_R) - x_3(0)}{t_R} \right]. \tag{23}$$

The SMC design steps are the same as in the previous section. This structure can be named as PI(propose)-SMC and shown in Fig. 10.

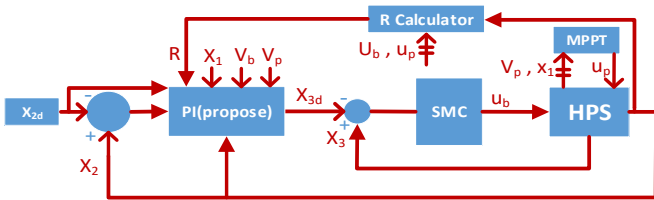


Fig. 10. Structure of PI (propose)-SMC.

#### 4. SIMULATION RESULTS

MATLAB environment is used to simulations. The HPS parameters are in accordance with Table 1 and 2. The MPPT and the performance of the proposed controller for the load voltage tracking are examined in two simulations.

##### 4.1 MPPT Simulations

In this case, the simulation investigates two PV characteristics: irradiance and temperature changes. The profile of solar irradiance and temperature are shown in Fig. 11.

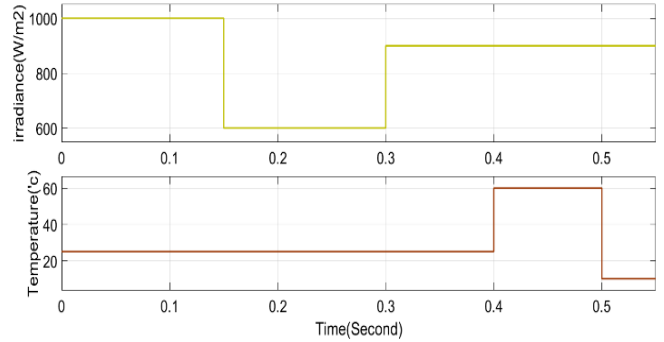


Fig. 11. Variation profile of solar temperature and irradiance.

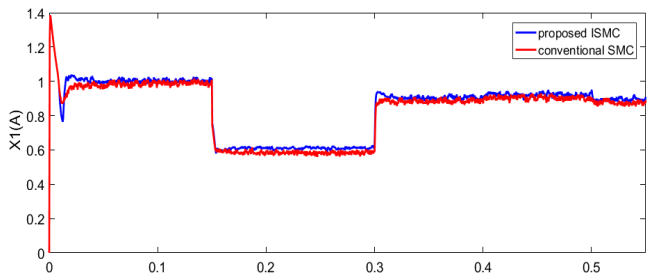
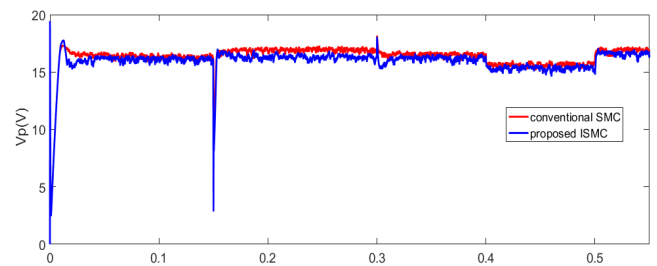
Initially, the Boost converter elements are considered ideal, and the performance of the proposed controller and conventional controller are compared. Then, the resistance of an inductor ( $R_{lp}$ ) is 1.5 ohms and repeats the simulation.

Table 1. Parameters description.

Symbol	Value	Symbol	Value
$V_b$	12V-7Ah	$K_s$	0.4
$L_b$	5mH	$K_{p1}$	0.8
$F_{switching}$	31.25kHz	$K_{i1}$	0.005
SW1, 2, 3	IRF540	$K$	0.02
$L_p$	5mH	$K_i$	0.0002
$C$	470 $\mu$ f	$t_R$	1 $\mu$ sec
		$t_d$	1.4 $\mu$ sec

Table 2. PV Parameters.

Symbol	Value	Description
$V_{oc}$	19.7V	
$I_{sc}$	1.45A	
$V_{MPP}$	16.2V	$\lambda=1000 \text{ W/m}^2$ & $T=298^\circ\text{K}$
$I_{MPP}$	1A	$\lambda=1000 \text{ W/m}^2$ & $T=298^\circ\text{K}$
$K_1$	0.3	



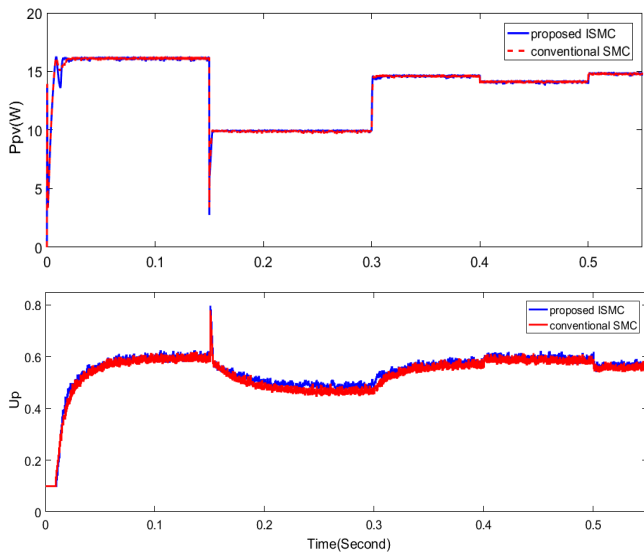


Fig. 12. The time response of PV when the boost converter is ideal.

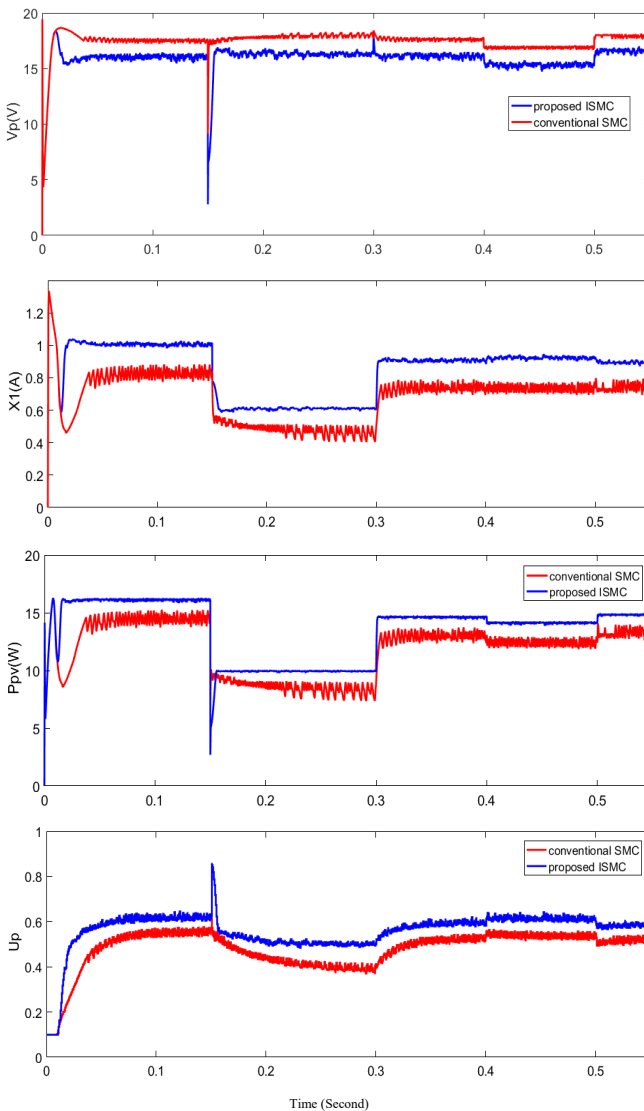


Fig. 13. The time response of PV when  $R_{lp} = 1.5 \Omega$ .

Due to Fig.12, the results show that the proposed ISMC and the conventional SMC are able to track MPP when the boost converter elements are considered ideal, but when these elements are considered reality, according to Fig. 13, the conventional SMC is not able to track MPP, while the extraction of the maximum power can be achieved robustly even can in the presence of climate (temperature or irradiance) or load changes by the proposed controller.

#### 4.2 Load Voltage Tracking Simulations

In this case, the desired output voltage ( $x_{2d}$ ) is 35 V and the PV irradiance is 1000 W/m<sup>2</sup> and the temperature is 298°K and at MPPT,  $V_p=16.2v$ ,  $x_1=1A$ . To illustrates the improvement of the dynamic response, the PI(propose)-SMC controller is compared with the PI-SMC controller. The response of both structures with the same control coefficients are compared as the sudden changes in the load from 100 ohms to 40 ohms and at 0.15 seconds when the load resistance varies from 40 ohms to 100 ohms are shown in Fig. 14. Simulation results show that both approaches have zero steady state error. The SMC is able to react maintaining the design specifications in both cases.

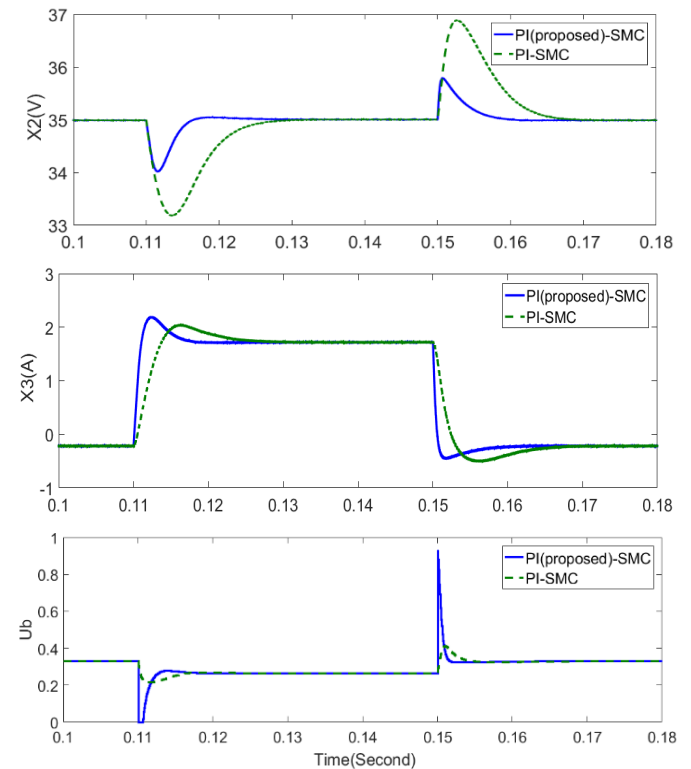


Fig. 14. The time response of load resistance variation.

However, the proposed control approach has better transient response.

### 5. EXPERIMENTAL VALIDATION

To verify the robustness of the proposed controller, the experimental configuration is set up as shown in Fig. 15, where specifications of the system are shown in Table 1 and 2. The proposed controller is implemented on SPARTAN XC3S400 chip. The PV voltage ( $V_p$ ) and current ( $x_1$ ), battery

voltage ( $V_b$ ) and current ( $x_3$ ) and load voltage ( $x_2$ ) are sent to the A/D pins of the chip. Afterward, the control signals ( $u_p$  and  $u_b$ ) are calculated and then, a PWM signal in 31250 Hz is directly generated to control the switches of the HPS. The control objectives are: load voltage regulation to 35 V; the PV irradiance is 1000 W/m<sup>2</sup> and the temperature is 298°K with in MPPT,  $V_p=16.2v$ ,  $x_1=1A$ . The resistance of the load varies directly from 50 to 100  $\Omega$ , and vice versa. Fig. 16 shows the voltage and current of the load unit. The first transient corresponds to load variation from 50 to 100  $\Omega$ , and the last transient corresponds to load variation from 100 to 50  $\Omega$ . It can be seen that the PI(propose)-SMC is able to track the reference voltage of the load with a reasonable performance, regardless of the load variation. The load disturbance produces a maximum transient deviation of the load voltage below 4%, which is rejected in less than 25 ms. The load voltage returns to 35 V after a fast transient state.

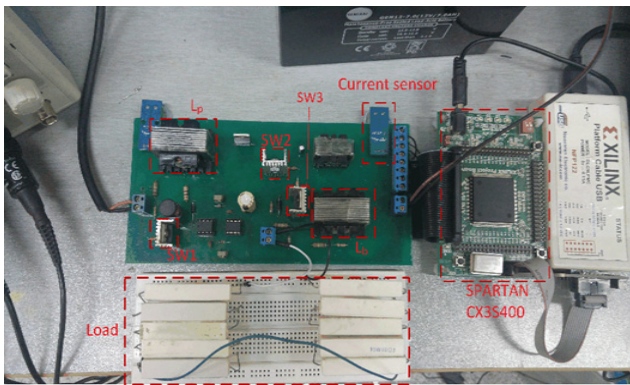


Fig. 15. Implementation of the closed-loop system.

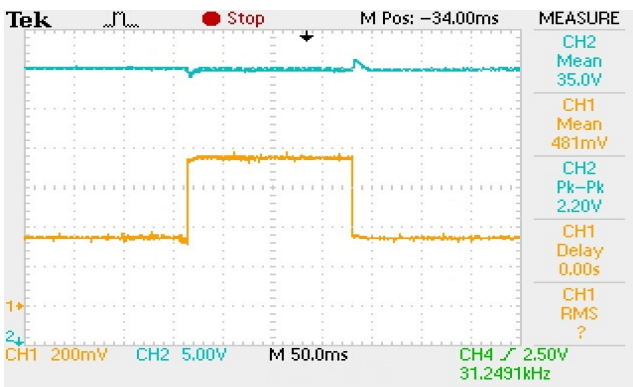


Fig. 16. Transient response with the load resistor (R) varying periodically stepwise between 50 and 100  $\Omega$ . CH1 (Bottom) load current (200 mA/div). CH2 (Top) load voltage (5V/div).

Fig. 17 shows the battery current. It can be realize that when the load resistance is increased from 50 to 100  $\Omega$ , the required power is lower than the PV power. In this condition, the sign of the battery current is negative. Fig. 18 presents the PV current ( $x_3$ ). It can be observed that the proposed ISMC regulates the PV current to  $I_{mppt}$  without steady-state error. The settling time of the PV current ( $x_3$ ) is about 25 ms. This tracking performance can maximize the extracted PV power. Experimental waveforms of the PV and battery voltages are shown in Fig. 19. It can be seen that the PV voltage is nearly

constant, while the battery voltage exhibits high variation due to the internal resistance. In the charge state, the battery voltage is higher than the nominal voltage. It can be concluded that the proposed system is robust with respect to PV voltage variation. Moreover, since the voltage of the battery changes due to the internal resistance, the proposed system is also robust toward battery voltage variations.

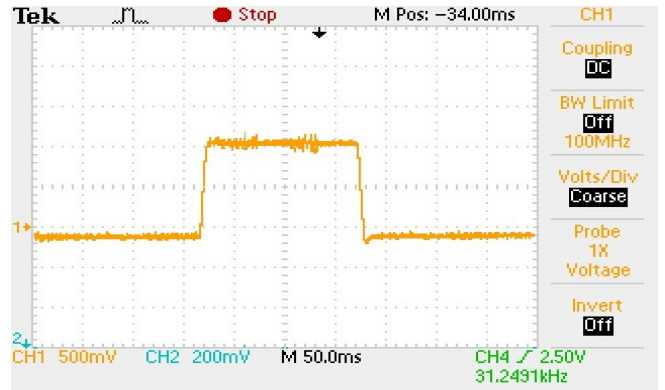


Fig. 17. Transient response with the load resistor (R) varying periodically stepwise between 50 and 100  $\Omega$ . CH1: battery current ( $x_3$ ) (500 mA/div).

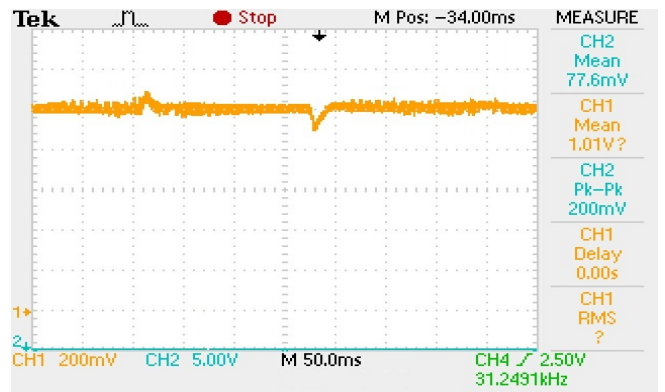


Fig. 18. Transient response with the load resistor (R) varying periodically stepwise between 50 and 100  $\Omega$ . CH1: Pv current ( $x_1$ ) (200 mA/div).

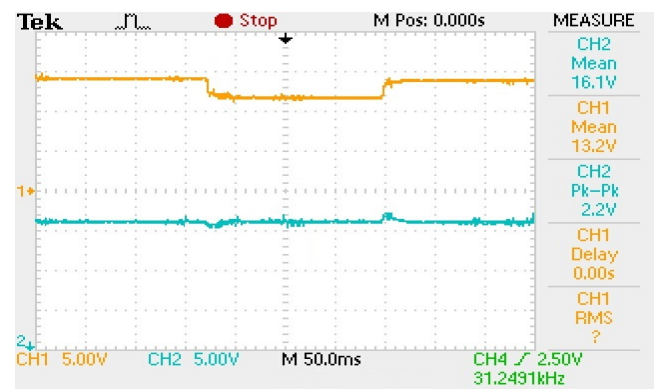


Fig. 19. Transient response with the load resistor (R) varying periodically stepwise between 50 and 100  $\Omega$ . CH1 (Top) battery voltage ( $V_b$ ) (5 V/div). CH2 (Bottom) PV voltage ( $V_p$ ) (5 V/div).

## 6. CONCLUSIONS

The nonlinear control of a HPS system and the improvement of the dynamic response have been analyzed in this study. The comparison between the responses of the conventional SMC and the proposed ISMC are shows that the conventional controller is not able to track MPP when the boost converter elements are considered reality, while the proposed controller can accurately track the MPP and therefore the conventional SMC is not an acceptable choice for MPPT. To adjust the load voltage to the desired value, BDC is driven with a double-loop controller. Asymptotic stability of the proposed controller system is ensured via Lyapunov theory. To improve the dynamic response of the system, the load resistance is calculated and placed in the outer loop, which is a PI (proposed) controller. The comparison between the responses of the PI-SMC and PI(proposed)-SMC shows that the proposed controller exhibits fast transient that corresponds to step changes in load resistance.

## REFERENCES

- Ahmad, H. B., Ahmed, M. K., Almoataz Y. A. (2014). Single-diode model based Photovol-taic module: Analysis and comparison approach. *Electric Power Components and Systems*, 42(12), 1289-1300.
- Ahmed, J. and Salam, Z. (2016). A Modified P&O Maximum Power Point Tracking Method With Reduced Steady-State Oscillation and Improved Tracking Efficiency. *IEEE Transactions Sustainable Energy*, 7(4), 1506 –1515.
- Algazar, M. M., Al-Monier, H., El-Halim, H. A., and Salem, M. E. E. K. (2012). Maximum power point tracking using fuzzy logic control. *International Journal of Electrical Power and Energy Systems*, 39(1), 21–28.
- Azzouzi, M. (2013). Optimization of Photovoltaic Generator by Using P&O Algorithm under different weather conditions. *Journal of Control Engineering & Applied Informatics*, 15(2), 12-19.
- Bahmanpour, M., Koofigar, H. R., Delshad, M., Tosifian, M. H. (2018). Design and Implementation of Robust Nonlinear Controller for Hybrid Power Sources with Considering Power Losses. *International Journal of Renewable Energy Research*, 8(3), 1411-1419.
- Belkaid, A., Gaubert J. P., Gherbi. A. (2016). An Improved Sliding Mode Control for Maximum Power Point Tracking in Photovoltaic Systems. *Journal of Control Engineering & Applied Informatics*, 18(1), 86-94.
- Dragomir, T.L., Petreus, D.M., Petcut, F.M., Ciocan, I.C. (2010). Comparative analysis of identification methods of the photovoltaic panel characteristics. *IEEE International Conference on Automation Quality and Testing Robotics*, 1-6.
- Elgendy, M. A., Zahawi, B., and Atkinson, D. J. (2015). Operating Characteristics of the P&O Algorithm at High Perturbation Frequencies for Standalone PV Systems. *IEEE Transactions Energy Conversion*, 30(1), 189–198.
- El Fadil, H. and Giri, F. (2011). Climatic sensorless maximum power point tracking in PV generation systems. *Control Engineering Practice*, 19(5), 513–521.
- Emadi, A. (2004). Modeling and analysis of multiconverter DC power electronic systems using the generalized state-space averaging method. *IEEE Transactions on Industrial Electronics*, 51(3), 661–668.
- Etxeberria, A., Vechiu, I., Camblong, H., Vinassa, J.-M. (2011). Comparison of Sliding Mode and PI Control of a Hybrid Energy Storage System in a Microgrid Application. *Energy Procedia*, 12, 966-974.
- Ghassami A.A., Sadeghzadeh S.M., Soleimani A. (2013). A high performance maximum power point tracker for PV Systems, *Electr. Power Energy Syst.* 53, 237-243.
- Khabbazi, N. S., Vali, A. R., and Behnamgol, V. (2017). Control of a Photovoltaic/Battery hybrid power source using the algorithm Super Twisting. *International Journal of Engineering Education*, 9(2).
- Killi, M. and Samanta, S. (2015). Modified Perturb and Observe MPPT Algorithm for Drift Avoidance in Photovoltaic Systems. *IEEE Transactions on Industrial Electronics*, 62(9), 5549–5559.
- Koofigar, H. (2016). Adaptive robust maximum power point tracking control for perturbed photovoltaic systems with output voltage estimation. *ISA Transactions*, 60, 285-293.
- Lin, B. (2000). Conceptual design and modeling of a fuel cell scooter for urban Asia. *Journal of Power Sources*, 86(1), 202-213.
- Mojallizadeh, M. R. and Badamchizadeh, M. A. (2016). Adaptive Passivity Based Control of a Photovoltaic/Battery Hybrid Power Source via Algebraic Parameter Identification. *IEEE Journal Photovoltaics*, 6(2), 532-539
- Mojallizadeh, M. R. and Karimi, B. (2014). Nonlinear control of a satellite power system based on the sliding mode control. *ISRN Aerospace engineering*, DOI: <http://dx.dio.org/10.1155/2013/253564>.
- Mojallizadeh, M. R. and Karimi, B. (2014). Nonlinear Control of a Photovoltaic/Battery Hybrid Power System, Based on the Sliding Mode Control. *Iranian electric industry. Journal of Quality and productivity*, 2(4), 30–40.
- Murtaza, A.F., Sher, H.A., Chiaberge M., Boero D., De Giuseppe M., Addoweesh K.E. (2012). A novel hybrid MPPT technique for solar PV applications using perturb & observe and fractional open circuit voltage techniques. *15th International Symposium on Mechatronika*, 5th-7<sup>th</sup> December, Prague, Czech, pp. 1-8.
- Park, H., Kim, Y. J. and Kim, H. (2016). PV Cell Model by Single-diode Electrical Equivalent Circuit. *Journal of Electrical Engineering and Technology*, 11(5), 1323-1331.
- Petcut, F., Dragomir, T.L. (2010). Solar Cell Parameter Identification Using Genetic Algorithms. *Journal of Control Engineering & Applied Informatics*, 12(1), 30-37.
- Sauer, K., Roessler, T., and Hansen, C. (2015). Modeling the irradiance and temperature dependence of photovoltaic modules in PVsyst. *IEEE Journal of Photovoltaics*, 5(1), 152–158.
- Sher, H.A., Murtaza, A.F., Noman, A., Chiaberge M., De Giuseppe M., Addoweesh K.E. (2015). A New Sensorless Hybrid MPPT Algorithm Based on Fractional Short-Circuit Current Measurement and P&O MPPT.

- IEEE Transactions on Sustainable Energy*, 6(4), 1426-1434.
- Syafaruddin, Karatepe, E. and Hiyama, T. (2012). Performance enhancement of photovoltaic array through string and central based MPPT system under non-uniform irradiance conditions. *Energy Conversion and Management*, 62, 131–140.
- Tan, S., Lai, Y. M., and Tse, C. K. (2008). General Design Issues of Sliding-Mode Controllers in DC–DC Converters. *IEEE Transactions on Industrial Electronics*, 55(3), 1160-1174.
- Thounthong, P. (2011). Model Based-Energy Control of a Solar Power Plant With a Supercapacitor for Grid-Independent Applications. *IEEE Transactions Energy Conversion*, 26(4), 1210-1218.
- Tofighi, A. and Kalantar, M. (2011). Power management of PV/battery hybrid power source via passivity based control. *Renewable Energy*, 36, 2440–2450.
- Xu, Z., Yang, P., Zhou, D., Li, P., Lei, J., and Chen, Y. (2015). An Improved Variable Step Size MPPT Algorithm Based on INC. *Journal of Power Electronics*, 15(2), 487-496.